Available online at www.sciencedirect.com
ScienceDirect
Comput. Methods Appl. Mech. Engrg. 279 (2014) 46–65
Computer methods in applied mechanics and engineering
www.elsevier.com/locate/cma

3D generation of realistic granular samples based on random fields theory and Fourier shape descriptors

Guilhem Mollon[a,*], Jidong Zhao[b]

[a] *LaMCoS, CNRS UMR 5259, INSA Lyon, Université de Lyon, Campus LyonTech la Doua, Bâtiment Jean d'Alembert, 18/20 rue des Sciences, 69621 Villeurbanne cedex, France*
[b] *Department of Civil and Environmental Engineering, Hong Kong University of Science and Technology, Clearwater Bay, Kowloon, Hong Kong*

Received 29 October 2013; received in revised form 5 March 2014; accepted 11 June 2014
Available online 18 June 2014

Abstract

The inability of simulating the grain shapes of granular media accurately has been an outstanding issue preventing particle-based methods such as discrete element method from providing meaningful information for relevant scientific and engineering applications. In this study we propose a novel statistical method to generate virtual 3D particles with realistically complex yet controllable shapes and further pack them effectively for use in discrete-element modelling of granular materials. We combine the theory of random fields for spherical topology with a Fourier-shape-descriptor based method for the particle generation, and develop rigorous solutions to resolve the mathematical difficulties arising from the linking of the two. The generated particles are then packed within a prescribed container by a cell-filling algorithm based on Constrained Voronoi Tessellation. We employ two examples to demonstrate the excellent control and flexibility that the proposed method can offer in reproducing such key characteristics as shape descriptors (aspect ratio, roundness, sphericity, presence of facets, etc.), size distribution and solid fraction. The study provides a general and robust framework on effective characterization and packing of granular particles with complex shapes for discrete modelling of granular media.

Keywords: Granular media; Discrete modelling; Particle shape generation; Particle packing; Random fields; Constrained Voronoi tessellation

1. Introduction

Granular materials are of primary interest for a wide range of industrial applications, including civil and chemical engineering, powders and pharmaceutical industries, mining and energy industries. They are meanwhile topics of interest for researchers across communities of granular physics, geophysics, tribology, nanoparticles and colloïds sciences. In the simulation and analysis of granular media, Discrete Element Method (DEM) has become a standard computational tool now. Early DEM studies on granular materials have considered circular or spherical particles due primarily to the simplicity and convenience in terms of contacts detection and repulsive forces computation [1].

* Corresponding author. Tel.: +33 781218101; fax: +33 478890980.
E-mail address: guilhem.mollon@gmail.com (G. Mollon).

http://dx.doi.org/10.1016/j.cma.2014.06.022
0045-7825/

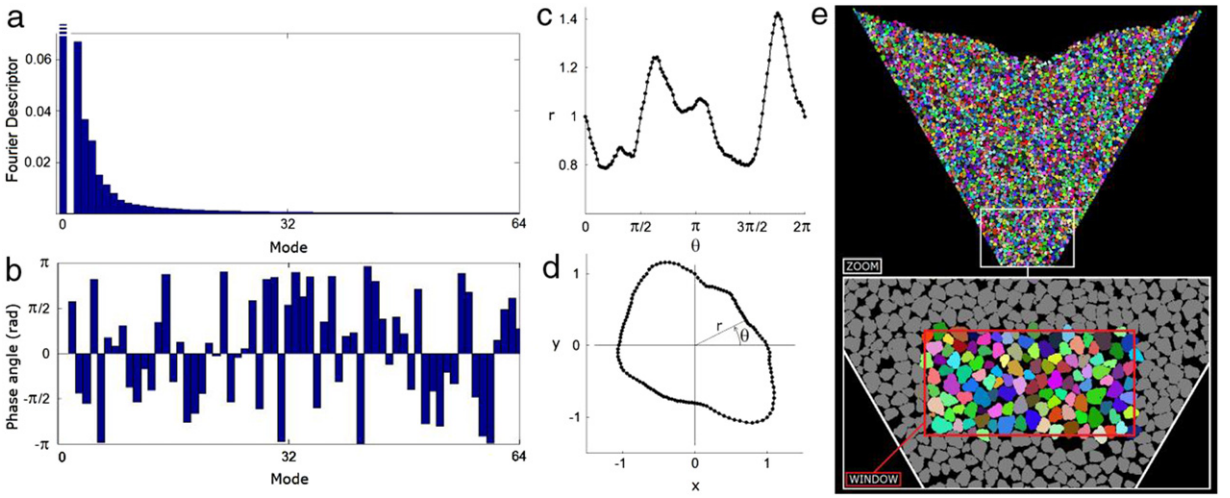

Fig. 1. Existing method for 2D generation of random particles [10,4]: a. Input Fourier spectrum; b. Random phase angles; c. Random signal; d. Same signal expressed in a polar frame; e. Application to the simulation of a 2D hopper flow.

It has become increasingly clear that these oversimplifications of particle shape in DEM modelling cannot provide adequately accurate and quantitative predictions on the behaviour of granular materials, and improved consideration of the realistic shape of granular particles has become a current trend. To this end, various non-circular shapes have been proposed to approximate the real shape of particles, ranging from clusters of discs or spheres (e.g. [2–9]), polygons, ellipses [10] and polyarcs to super-ellipsoids [11–13], cylinders [14] and polyhedrons or sphero-polyhedrons [15–22]. Though they have helped to gain various improvements on the understanding of granular behaviour, these approaches remain to be too simplified approximations to provide accurate description of the real shape of particles. Due to these geometric simplifications, various assumptions with obscure physical meanings have to be made on contact parameters (such as friction, stiffness, viscosity) in DEM simulations and need to be calibrated by back analysis, which brings in more or less phenomenological ingredients into DEM. The DEM simulations based on these simplified considerations remain a long way from providing quantitative predictions on the real behaviour of granular materials. There is a need for systematic approaches to be developed to effectively represent the realistic geometric characteristics of granular particles before incorporation in DEM modelling.

In this study, we aim to develop a novel statistical approach to solve the above issues. In particular, we identify statistical properties representing the unique shape characteristics of a granular material to provide faithful reference for generating realistic three-dimensional packing of particles for DEM modelling. The study is based on an early two dimension work by the authors [23] wherein the concept of Fourier descriptors was employed. Fourier shape descriptors were first introduced in [24] for particle shape characterization and were further applied by several authors to sand characterization (see, e.g. [25]). It was shown that the average normalized Fourier spectrum (Fig. 1a) of the 2D projected contours (expressed in polar coordinates) of a family of particles may embody a relevant signature of the shape features of these particles. The amplitude of Mode D_2 of such a spectrum is a good descriptor of the particle elongation, the next few modes contain information on the main shape irregularities, and the high-frequency modes describe the surface roughness of the particle. The normalized spectrum of a population of granular particles is rather easy to obtain experimentally, using, for example, micro-photographs coupled with simple image treatment algorithms and discrete Fourier transform [25]. A particular innovation in [23] was to reverse the concept, by using such a spectrum as the starting point for generating random particles with prescribed shape features. This was done by performing an inverse Fourier transform on a chosen spectrum (Fig. 1a), with the randomness being introduced by means of random phase angles for each Fourier mode (Fig. 1b). The generated 2D particles were then packed in a chosen virtual container with a prescribed granular density based on a constrained Voronoi tessellation approach. The working program (coded in a MATLAB and available for free download at http://guilhem.mollon.free.fr) can now help us generate a packed 2D granular sample with perfectly controlled properties including size distribution, elongation, roundness, circularity, regularity, orientation anisotropy and void ratio. This program was successfully applied to the modelling of a 2D sand flow through a wedge-shaped hopper (see Fig. 1e and Refs. [4,26]).

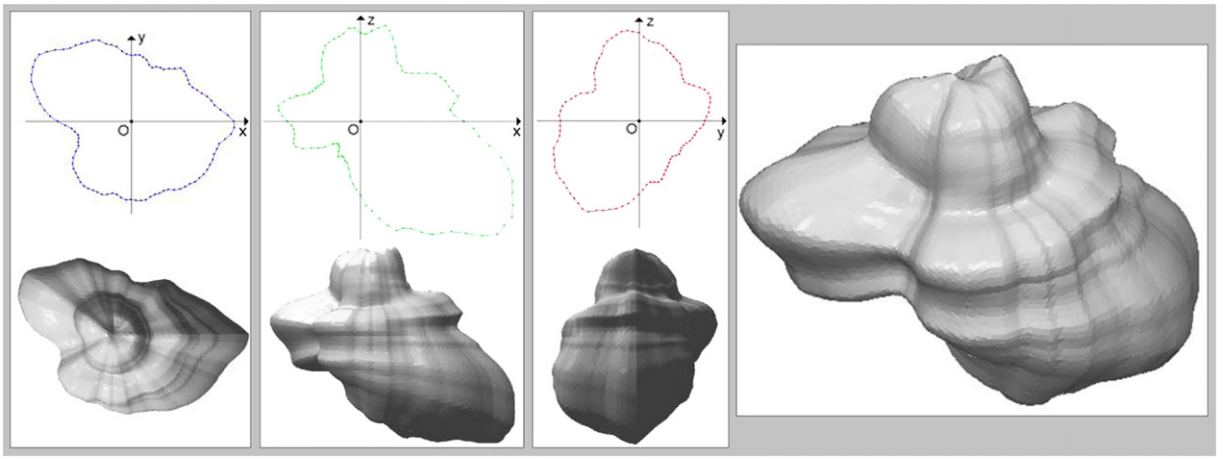

Fig. 2. Existing method for 3D generation of random particles, based on three 2D contours used as orthogonal cross-sections [13].

These previous studies, however, were limited to two-dimensional problems only and can be hardly useful for the prediction of three-dimensional problems in the real world. To resolve this issue, we proposed a quick solution in a more recent paper [27]. It was based on a direct extension of the 2D framework proposed in [23] by choosing three random 2D contours (based on a desired spectrum) as the three orthogonal cross-sections of a hypothetical grain (Fig. 2) and developing a complicated revolving–stretching–morphing technique to extrapolate the whole external surface of the 3D grain from these cross-sections. A comparison between 2D projections of real targeted grains and the generated particles proved that the method may be accurate but may still exhibit three noticeable drawbacks: (i) the extrapolation technique did not lead to an isotropic distribution of the shape irregularities (see Fig. 2); (ii) this method was not able to reproduce the "facetted" shapes (plateau surface) that characterize many granular particles; and (iii) the three chosen 2D contours may be too arbitrary and affect the morphology of the generated 3D in a unrealistic manner. We hereby will solve these issues by proposing a different and more general framework on realistic 3D particle generation, based on the random fields theory in conjunction with Fourier shape descriptors. We also tackle the problem of packing the generated 3D grains in an arbitrary 3D container and creating complex 3D granular samples with controlled shape and size distribution features. The proposed framework is expected to be of potential benefit to the future developments of DEM utilizing such level of details.

2. Particle generation

2.1. The concept of discrete random field

In line with our previous studies [27], the generation method presented in this section is restricted to the so-called "star-like" shapes. With a "star-like" shape particle, it is always possible to define a centre O for which, in any direction of space defined by two angles (θ, φ), there is exactly one intersection with the particle external surface at a distance R from this centre (Fig. 3a). Thus, in this class of shapes (which covers most cases of the granular materials encountered in scientific and industrial applications), the external surface of a particle can be entirely defined by a continuous function expressed in terms of the following "radius" from the centre:

$$R(\theta, \varphi) \quad \text{with } 0 \leq \theta \leq 2\pi \quad \text{and} \quad 0 \leq \varphi \leq \pi. \tag{1}$$

This function has a proper periodic property to be defined on a spherical topology. In the simplest case of a constant R, the represented particle is a perfect sphere. On the other hand, if one wishes to generate random shapes with controlled features, it might be interesting to pay attention to the mathematical properties of this function, and to consider it as a random field defined on a spherical domain. In this latter case, the local value of the function R for any point (θ, φ) is considered as a random variable, with specified mean value, standard deviation and probability density function. In addition, for any couple of points $\left(P_{i_1}, P_{i_2}\right)$, the two random variables $\left(R_{i_1}, R_{i_2}\right)$ are linked by a coefficient of

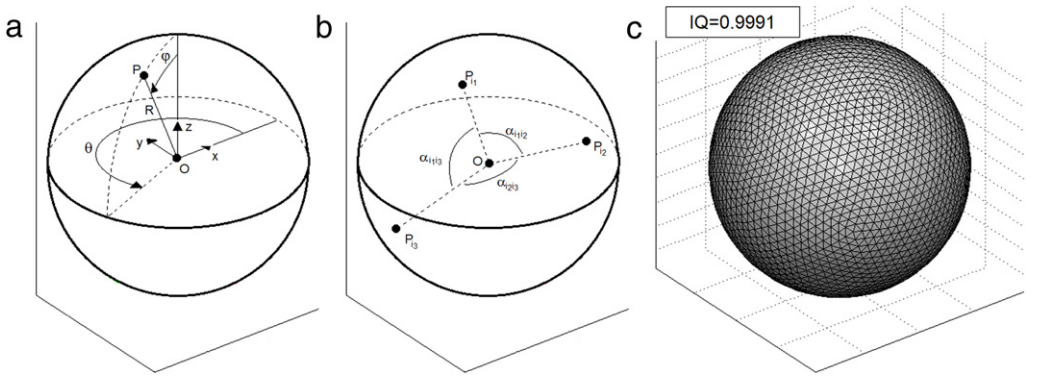

Fig. 3. Description of 3D shape: a. Classical spherical frame; b. Angles α between different points; c. Geodesic structure used to approximate star-like shapes.

correlation $\rho_{i_1 i_2}$ which depends on the positions of the two points $\left(P_{i_1}, P_{i_2}\right)$:

$$\rho_{i_1 i_2} = \rho\left(\theta_{i_1}, \varphi_{i_1}, \theta_{i_2}, \varphi_{i_2}\right). \tag{2}$$

In order for the shape features to be statistically isotropic and invariant with respect to the angular position, the general formulation given in Eq. (2) should be made more specific such that the correlation coefficient $\rho_{i_1 i_2}$ is independent from the absolute positions of P_{i_1} and P_{i_2}, and is only a function of the angle $\alpha_{i_1 i_2} = \widehat{P_{i_1} O P_{i_2}}$ between the two points (Fig. 3b) :

$$\rho_{i_1 i_2} = \rho\left(\alpha_{i_1 i_2}\right). \tag{3}$$

This function $\rho(\alpha)$ is called autocorrelation function, and describes the way the correlation between the radiuses of two points evolves with their angular distance. The random field can then be entirely described by the probability density function of the radius (PDF, which will be chosen as Gaussian for the sake of simplicity in the remainder of this paper) and the autocorrelation function which should be carefully chosen to properly describe the random patterns of the shape irregularities.

For practical applications, it is relatively easier to work with a discrete random field rather than a continuous one. To this end, we consider a discretization of the surface of the unit sphere, based on the concept of geodesic structures we presented in [27]. In this discretization scheme, the external surface of the sphere is represented by a collection of 5130 triangular facets, bounded by the segments joining 2562 points. As shown in Fig. 3c, a surface so constructed with a constant radius is a good approximation of a sphere (Isoperimetric quotient of 0.9991 instead of 1). It can also approximate any star-like shape if the collection of radiuses R_i $(1 < i < 2562)$ is well chosen. In the remainder of the paper, the subscript i will always denote a direction of space, i.e. the direction of one of the 2562 vertices of the geodesic structure, with its own radius R_i. All the angular coordinates (θ_i, φ_i) of these 2562 points are well known, and the angles $\alpha_{i_1 i_2}$ between any couple of points can be computed easily by basic geometry, which leads to the following matrix of angles:

$$[\alpha] = \begin{bmatrix} \alpha_{11} & \cdots & \alpha_{1\,2562} \\ \vdots & \ddots & \vdots \\ \alpha_{2562\,1} & \cdots & \alpha_{2562\,2562} \end{bmatrix}. \tag{4}$$

Given an autocorrelation function $\rho(\alpha)$, it is possible to compute the correlation matrix that links the 2562 random variables R_i:

$$[\rho] = \rho([\alpha]) = \begin{bmatrix} \rho(\alpha_{11}) & \cdots & \rho(\alpha_{1\,2562}) \\ \vdots & \ddots & \vdots \\ \rho(\alpha_{2562\,1}) & \cdots & \rho(\alpha_{2562\,2562}) \end{bmatrix} = \begin{bmatrix} \rho_{11} & \cdots & \rho_{1\,2562} \\ \vdots & \ddots & \vdots \\ \rho_{2562\,1} & \cdots & \rho_{2562\,2562} \end{bmatrix}. \tag{5}$$

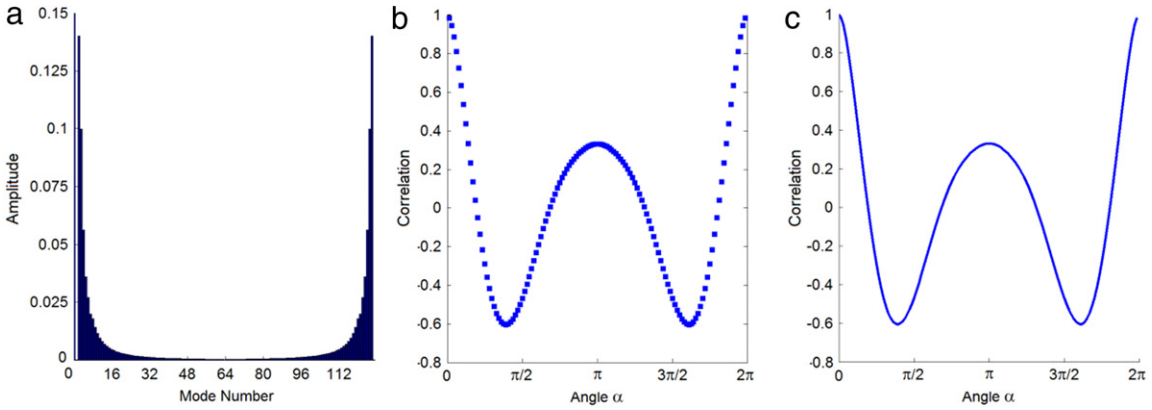

Fig. 4. a. Illustrative normalized and symmetric Fourier spectrum; b. Corresponding discrete autocorrelation function; c. Interpolated continuous autocorrelation function.

The above correlation matrix is the main tool for practical realization of the random fields on particle generation. In order for the 2562 radiuses to follow a classical Gaussian multivariate distribution (and thereby for the collection of radiuses R_i to be an actual discrete random field), the matrix $[\rho]$ needs to be symmetric definite positive, and all the diagonal terms ρ_{ii} should be equal to 1. Of the two conditions, the first one strongly restrains the choice of the autocorrelation function $\rho(\alpha)$ as will be further elaborated, while the second one only imposes $\rho(0) = 1$.

In this study, we further employ the Expansion Optimal Linear Estimation (EOLE) method first proposed in [28]. This method enables us to generate random realizations of N multivariate Gaussian random variables $\{R\}$ defined by their $N \times 1$ vector of mean values $\{\mu\}$ and their $N \times N$ covariance matrix $[C]$ of the following general term:

$$C_{i_1 i_2} = \rho_{i_1 i_2} \cdot \sigma_{i_1} \cdot \sigma_{i_2} \tag{6}$$

where σ_i is the standard deviation of the random variable R_i. In the present case, we have $N = 2562$. A given random realization may be obtained by the following formula:

$$\{R\} = \{\mu\} + \sum_{j=1}^{2562} \xi_j \cdot \sqrt{\lambda_j} \cdot \left\{\Phi_j\right\}. \tag{7}$$

In this expression, λ_j is the jth eigenvalue of the covariance matrix $[C]$, $\left\{\Phi_j\right\}$ is the corresponding eigenvector, and ξ_j is a Gaussian random variable with zero-mean and unit-variance. In the sequel, the subscript j (with $1 \leq j \leq 2562$) will always be assumed to denote one of the eigenmodes of the covariance matrix. Eq. (7) makes it possible to create a random realization of a vector of correlated variables R_i directly by means of the uncorrelated random variables ξ_j which can be automatically generated by any commercial computational package (e.g. MATLAB, excel, etc.). However, it requires all the eigenvalues of $[C]$ to be positive, which is the reason why the covariance matrix (and in turn the correlation matrix) has to be symmetric definite positive.

2.2. Computation of the correlation matrix

In the 2D framework we proposed in [23], one of the main advantages lies in that the random particle shape features can be controlled by an input discrete Fourier spectrums, each mode of which describes the amplitude of the surface irregularities of a given spatial frequency. It enables one to use spectrums obtained from the experimental characterization of the target granular material grains, and meanwhile renders it possible to use tailor-made spectrums to investigate the influence of each class of particle irregularity. For these reasons, it would be desirable to be able to control the 3D particles with the same tool, i.e. a discrete Fourier spectrum. Fortunately, the theory of signal processing provides a direct relation between the Fourier spectrum and the autocorrelation function of a discrete 1D signal of zero mean, the latter being the inverse discrete Fourier transform of the power spectrum obtained from the former. More precisely, let us consider a Fourier spectrum of 64 independent modes of amplitudes D_k, with $0 \leq k \leq 127$ (Fig. 4a). The spectrum is normalized (i.e. $D_0 = 1$) and symmetric (i.e. $D_k = D_{128-k}$ for $2 \leq k \leq 64$), and the mode D_1 is

set to 0 by convention (see [23] for more details). Hence, this spectrum is controlled by 63 independent modes. The corresponding autocovariance function is then given by:

$$C(\alpha_m) = \sum_{k=1}^{127} D_k^2 \cdot e^{2i\pi m \frac{k}{128}} \quad \text{with } 0 \leq m \leq 127. \tag{8}$$

This autocovariance function is discrete, 2π-periodic, and is only known at given angles α_m:

$$\alpha_m = \frac{2\pi m}{128} \quad \text{with } 0 \leq m \leq 127. \tag{9}$$

The value of the autocovariance function at $\alpha_0 = 0$ corresponds to the variance σ^2 of the discrete signal, and the autocorrelation function (Fig. 4b) is thus given by:

$$\rho(\alpha_m) = C(\alpha_m)/C(\alpha_0) \quad \text{with } 0 \leq m \leq 127. \tag{10}$$

Finally, an equivalent continuous autocorrelation function can be obtained by simply interpolating the discrete one over the whole interval $[0, 2\pi]$ (Fig. 4c). This autocorrelation function describes a continuous 1D signal with zero mean and a standard deviation equal to:

$$\sigma = \sqrt{\sum_{k=1}^{127} D_k^2}. \tag{11}$$

Combining Eqs. (5) and (10) makes it possible to fill the matrix $[\rho]$ and further using Eq. (11) provides the matrix $[C]$. However, it appears that the matrix obtained by this procedure cannot be guaranteed to be definite positive and hence cannot be considered as an actual covariance matrix in the general case. This is because the spherical topology of the domain brings periodicities of different natures than those for a 1D signal (or even for a 2D signal defined on a plane square domain), and puts some strong restrictions on the valid autocorrelation functions to be used. It is hence not possible to apply Eq. (7) directly to the particle generation, and another way has to be found. We hereby propose a new method to overcome this difficulty. It takes advantage of the Fourier descriptors and is based on a controlled alteration of the $[C]$ matrix to render it definite positive without deteriorating its frequency properties. In this method, each Fourier mode is treated separately. For a given mode K, a unit spectrum is created with:

$$\begin{cases} D_k = 1 & \text{if } k = K \text{ or } k = 128 - K \\ & \text{with } 2 \leq k \leq 64 \\ D_k = 0 & \text{otherwise.} \end{cases} \tag{12}$$

Fig. 5a presents an example with $K = 5$. This unit spectrum, related to Fourier mode K, is first applied to the procedure described in Eqs. (8) and (10) to obtain the equivalent continuous autocorrelation function (Fig. 5b). Eqs. (5), (11) and (6) are then successively applied to build a matrix $[C]_K$. However this matrix does not possess the definite positive property for whatever the mode number K, and cannot yet be considered as a covariance matrix. Indeed, a computation of its eigenvalues $\{\lambda_j\}_K$ and the corresponding eigenvectors $\{\Phi_j\}_K$ shows that a large number of the eigenvalues are negative, and the observation sustains for any mode K. However, a close observation of the eigenvalues reveals that, for any K, there are always $2K + 1$ eigenvalues which are strongly dominant, i.e. they have very large positive values. All the others are either negative or positive but typically very small. Hence, we propose to consider that only these $2K + 1$ dominating eigenvalues (and their related eigenvectors) carry relevant information while the others are only marginally relevant and can be neglected. Based on this assumption, a new matrix $[C']_K$ is computed using the following formula:

$$[C']_K = [\Phi]_K \cdot [\lambda']_K \cdot [\Phi]_K^T. \tag{13}$$

In this expression, $[\Phi]_K$ is the square matrix consisting of the eigenvectors of $[C]_K$, and $[\Phi]_K^T$ is its transposed matrix; $[\lambda']_K$ is a diagonal matrix containing the eigenvalues of $[C]_K$, except that those eigenvalues λ_j that do not belong to the $2K + 1$ dominating group are set to zero. To sum up, the key processes of the proposed method includes (a) considering the matrix $[C]_K$; (b) identifying its meaningful eigenmodes; (c) "separating" them from the others, and

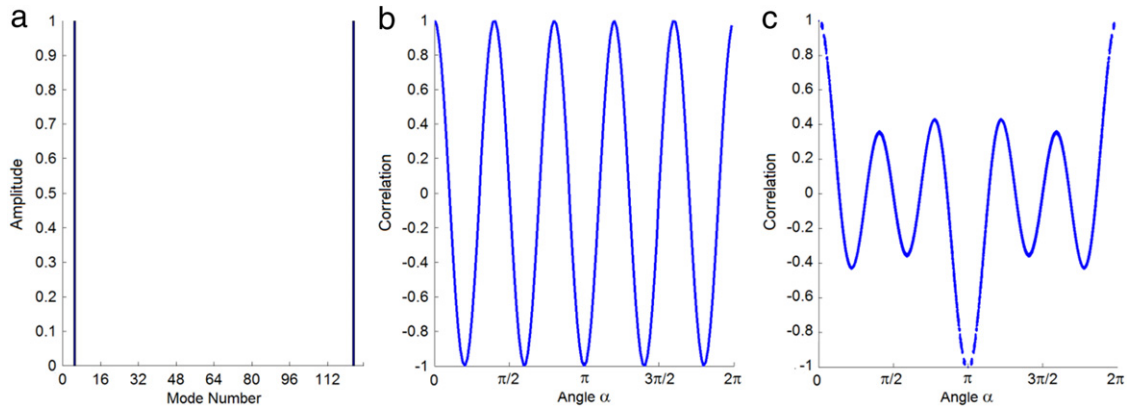

Fig. 5. Individual Fourier mode processing: a. Fourier spectrum with amplitudes of modes 5 and 123 set to 1; b. Corresponding continuous autocorrelation function; c. Cloud of points obtained when plotting the content of the corrected correlation matrix with respect to the one of the matrix of angles.

(d) reconstructing a cleaned matrix $\left[C'\right]_K$. The new matrix so obtained is always symmetric definite positive, and its diagonal values are all quasi-identical and very close to a certain value ε_K. This value is a side effect of the "cleaning" process, and is not relevant by itself. Thus, a valid correlation matrix may be obtained by simply computing:

$$\left[\rho'\right]_K = \frac{1}{\varepsilon_K} \cdot \left[C'\right]_K . \tag{14}$$

In Fig. 5c, one may observe a cloud of points obtained when plotting the 2562×2562 components of the new correlation matrix $\left[C'\right]_K$ with respect to those of the matrix of the angular distances $[\alpha]$. It appears that the initial autocorrelation function $\rho(\alpha)$ (which led to an invalid correlation matrix) has been somewhat replaced by a corrected autocorrelation function $\rho'(\alpha)$, which provides a valid correlation matrix and meanwhile preserves the frequency features as well as the physical significance of the original function.

When applied to all the modes K, the procedure described in Eqs. (12)–(14) helps to build a library of correlation matrices $\left[\rho'\right]_K$ (with $2 \leq K \leq 64$) of dimensions 2562×2562, each of which describes the correlation pattern of a given Fourier mode. This operation, which may be seemingly rather cumbersome due to the need of computing the eigenmodes of several large matrices, has only to be performed once since these matrices are only dependent on the positions of the 2562 points of the geodesic structure (Fig. 3c). The matrices can then be stored in an archive on the hard drive of a computer and be called when needed. For a given normalized and symmetric spectrum with amplitudes D_K (with $D_0 = 1$, $D_1 = 0$, and $D_K = D_{128-K}$ for $2 \leq K \leq 64$), a global matrix of covariance $\left[C'\right]$ may then be directly computed by a simple weighted sum of the individual correlation matrices related to each Fourier mode:

$$\left[C'\right] = \sum_{k=1}^{64} 2 \cdot D_K^2 \cdot \left[\rho'\right]_K . \tag{15}$$

This matrix is symmetric definite positive by construction and contains the individual frequency feature of each individual Fourier mode as well as the relative weights of all the modes provided by the input Fourier spectrum. It is thus expected to provide a good control over the random shape features of the particles, which can be randomly generated by the direct application of Eq. (7), only with $[C]$ being replaced by $\left[C'\right]$.

2.3. Analysis of the generated grains

For illustrative purpose, we consider a normalized Fourier spectrum with $D_0 = 1$, $D_1 = 0$, $D_2 = 0.075$, and a logarithmic decay (of base 2, see [23] for more details) with a parameter -1.6 for higher modes (i.e. $D_k = 2^{-1.6 \cdot log_2(k/2) + \log_2(D_2)}$ for $3 \leq k \leq 64$). This spectrum has been chosen here because it gives good visual results. Nevertheless any other spectrum may be used. Fig. 6 presents the respective roles of several modes within this spectrum. For each row of this figure, one or more modes of the spectrum is kept (shown in black) while the

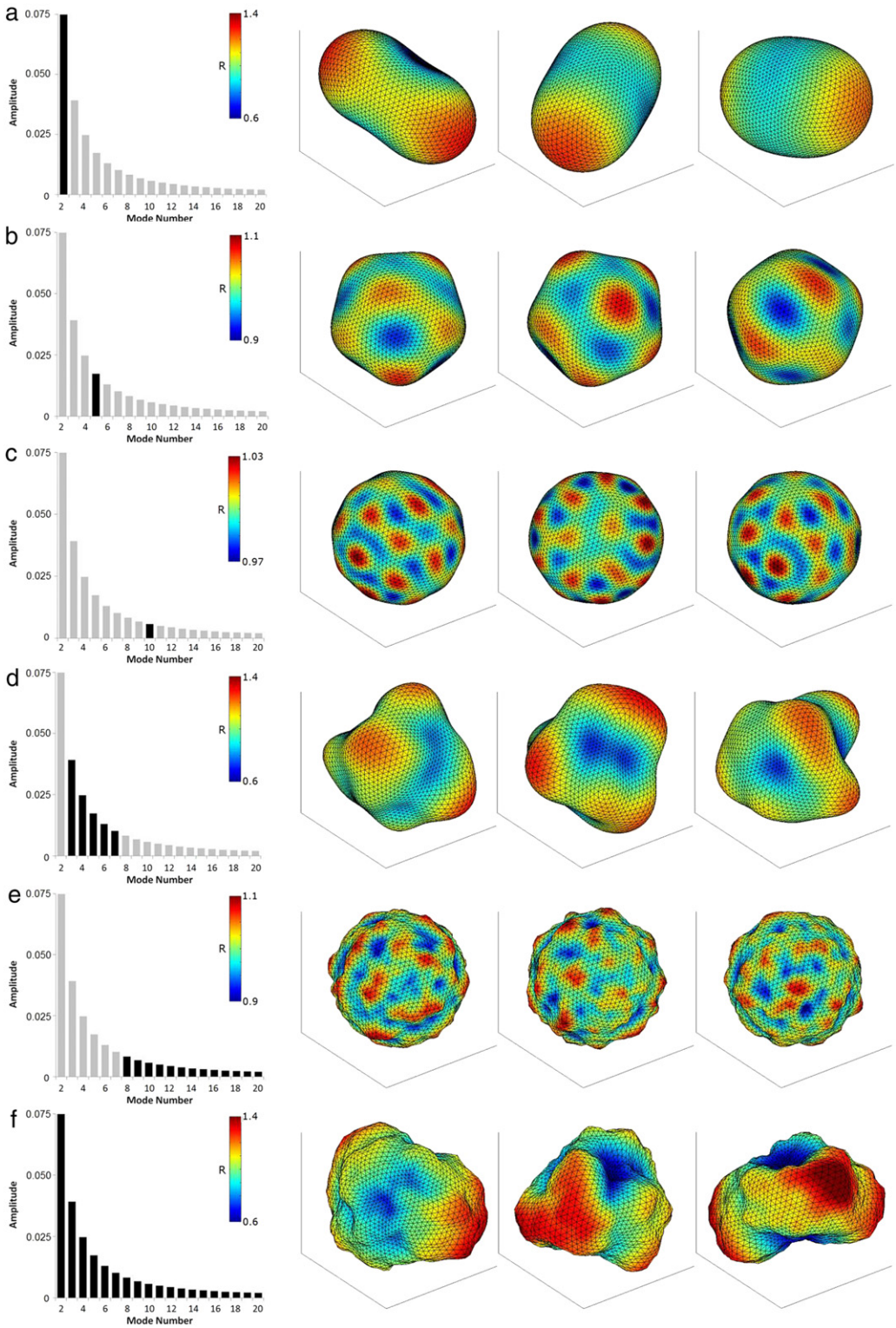

Fig. 6. Illustrative particles generated using the proposed framework. Left-hand: considered modes of an illustrative Fourier spectrum (in black, modes set to 0 are in grey); Right-hand: three random particles generated with this spectrum. a. Mode 2; b. Mode 5; c. Mode 10; d. Modes 3–7; e. All modes larger than 8; f. Full spectrum.

other modes are set to zero (shown in grey), and three particles are randomly generated with the resulting partial spectrum. For these generations, Eq. (7) has been used with the mean values $\{\mu\}$ equal to 1 for all the random variables composing $\{R\}$. This is necessary for the modes amplitude to be consistent, because the Fourier spectrums are normalized. If necessary, other sizes of particles may be obtained after the generation by simply applying a scaling factor to all the generated radiuses.

The first row of Fig. 6 presents the particles generated by the consideration of the mode D_2 only. It appears that these particles are very rounded and smooth but are somewhat elongated in a given direction. While the elongation is controlled by the value of D_2 in an average way, the randomness is preserved in terms of both amplitude (around this average) and direction. In the second and third rows of Fig. 6, modes 5 and 10 are respectively considered. Again, it appears that the particles generated are random, but exhibit a well-controlled periodicity and amplitude in their shape irregularities. The periodicity is controlled by the mode number and the amplitude by the mode value. The fourth and the fifth row of Fig. 6 consider different sets of modes, following the framework presented in [23]: modes D_3–D_7 for the fourth row, and modes $D_{>7}$ for the fifth row. Clearly, the modes D_3–D_7 provide control on the main irregularities of the shape without introducing any surface roughness, while the modes $D_{>7}$ provide a good control of the surface roughness without modifying the global spherical shapes of a particle. As a consequence, good control over a particle shape may be achieved by only tuning three parameters: D_2, D_3 (modes D_4–D_7 being obtained by logarithmic decay from D_3 with a parameter of -1.6), and D_8 (modes $D_{>8}$ being obtained by logarithmic decay from D_8 with a parameter of -1.6). Nevertheless, the separation between modes D_7 and D_8 is notably rather artificial, and more degrees of freedom may be used if a greater flexibility is needed. In the following demonstrative examples of the proposed method, the highest considered mode is Number 64, which corresponds to an angular period close to 5.6°. For a particle of average diameter D, the distance between two "peaks" of this mode is thus close to $D/20$. In the last row of Fig. 6, three particles are generated in consideration of the full spectrum, which demonstrates the capacity of the proposed method in characterizing the entire complexity of particle shapes.

Following this framework (i.e. controlling a spectrum with D_2, D_3 and D_8 only), it is instructive to perform a more quantitative study of the influence of these parameters on some more classical shape descriptors. If L, I, and S are used to denote respectively the longest, intermediate and smallest dimensions of a rectangular box containing exactly the particle (following the box-fitting method presented in [29]), we may define the following dimension ratios:

$$\text{Flatness} = \frac{S}{I} \tag{16}$$

$$\text{Elongation} = \frac{I}{L} \tag{17}$$

$$\text{Aspect ratio} = \frac{S}{L}. \tag{18}$$

In addition, we also define the following descriptors:

$$\text{Roundness} = \frac{\sum R_c}{n_c \cdot R_{insc}} \tag{19}$$

$$\text{Sphericity} = \sqrt{\frac{R_{insc}}{R_{circ}}} \tag{20}$$

$$\text{Isoperimetric quotient} = \frac{36\pi \cdot V^2}{A^3}. \tag{21}$$

In these expressions, R_{insc} and R_{circ} are the radiuses of the largest inscribed and the smallest circumscribed spheres of the considered particle, respectively. The terms R_c are the radiuses of the n_c overlapping spheres used to fill accurately the volume of the particle (following the ODEC framework presented in [3]), and V and A are respectively the volume and external area of the considered particle.

Figs. 7–9 present the influence on these six descriptors of D_2, D_3 and D_8, respectively. 2000 particles are generated for each case, and the average values (solid lines) and standard deviations (dot lines) of each descriptor are computed based on these samples. Each figure highlights the influence of a single parameter only (for example D_3 in Fig. 8),

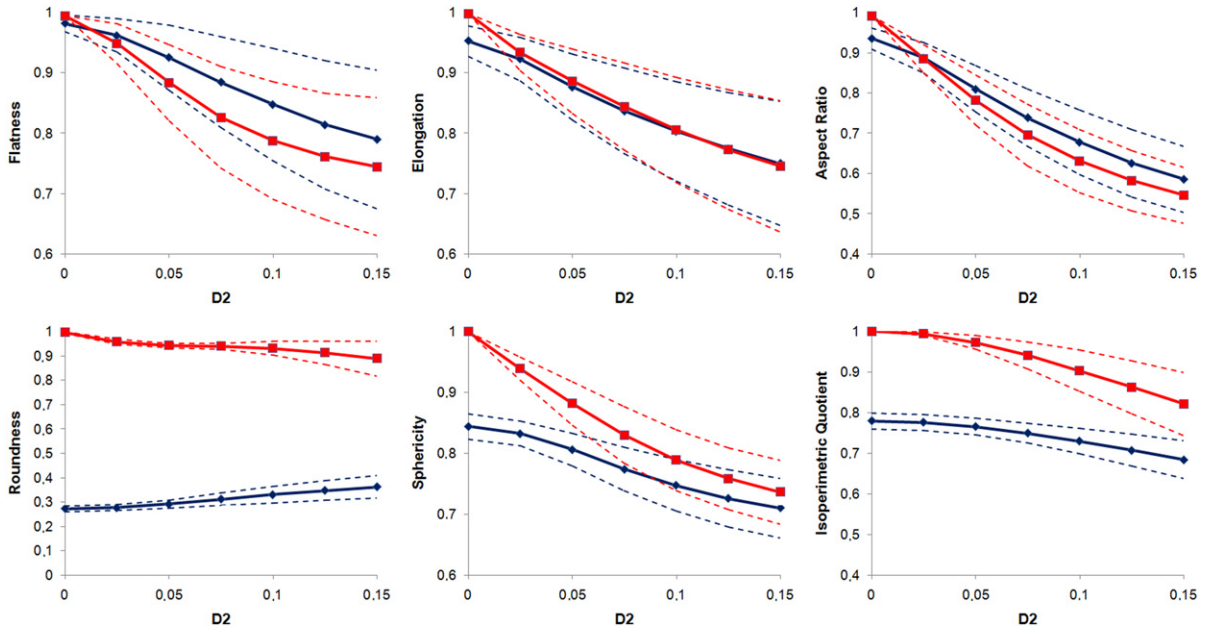

Fig. 7. Influence of the parameter D_2 on the Flatness, Elongation, Aspect Ratio, Roundness, Sphericity, and Isoperimetric Quotient of 2000 generated particles. Solid lines: mean values; Dotted lines: mean values $+/-$ one standard deviation. In blue: all other modes consistent with the spectrum of Fig. 6; In red: all other modes set to zeros. (For interpretation of the references to colour in this figure legend, the reader is referred to the web version of this article.)

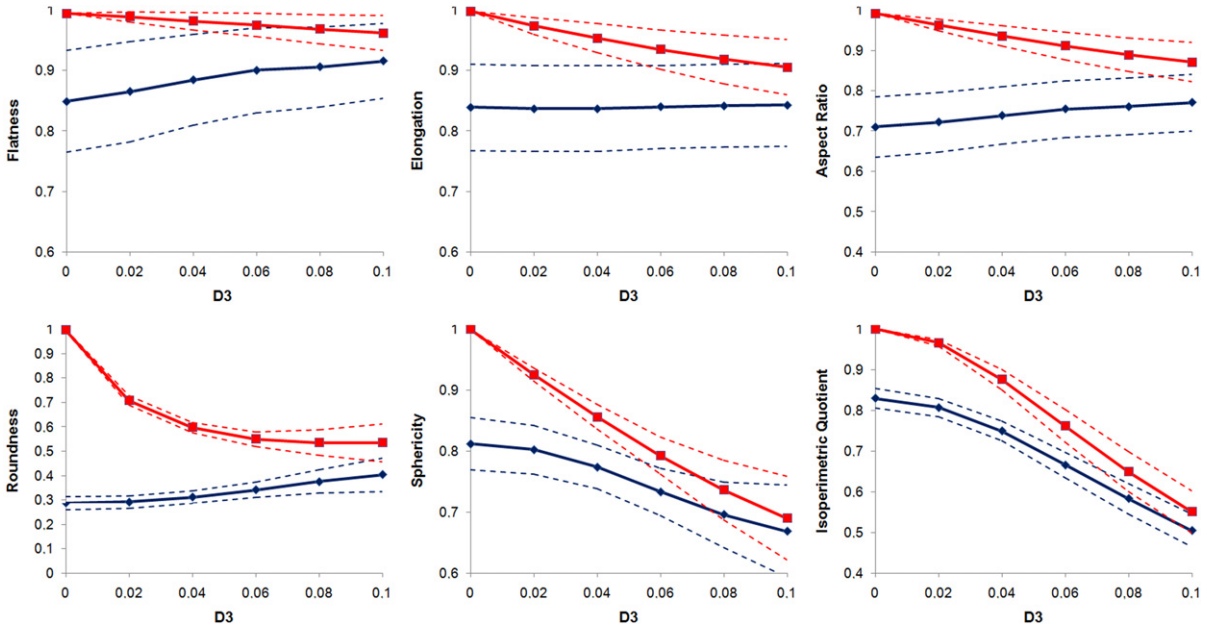

Fig. 8. Influence of the parameter D_3 (modes D_4–D_7 being related to D_3 by logarithmic decay) on the Flatness, Elongation, Aspect Ratio, Roundness, Sphericity, and Isoperimetric Quotient of 2000 generated particles. Solid lines: mean values; Dotted lines: mean values $+/-$ one standard deviation. In blue: all other modes consistent with the spectrum of Fig. 6; In red: all other modes set to zeros. (For interpretation of the references to colour in this figure legend, the reader is referred to the web version of this article.)

and two cases are considered for the other modes (D_2 and $D_{>7}$ in this case): identical values are used for them as in the illustrative spectrum in Fig. 6 (blue lines), or they are all set to zeros (red lines).

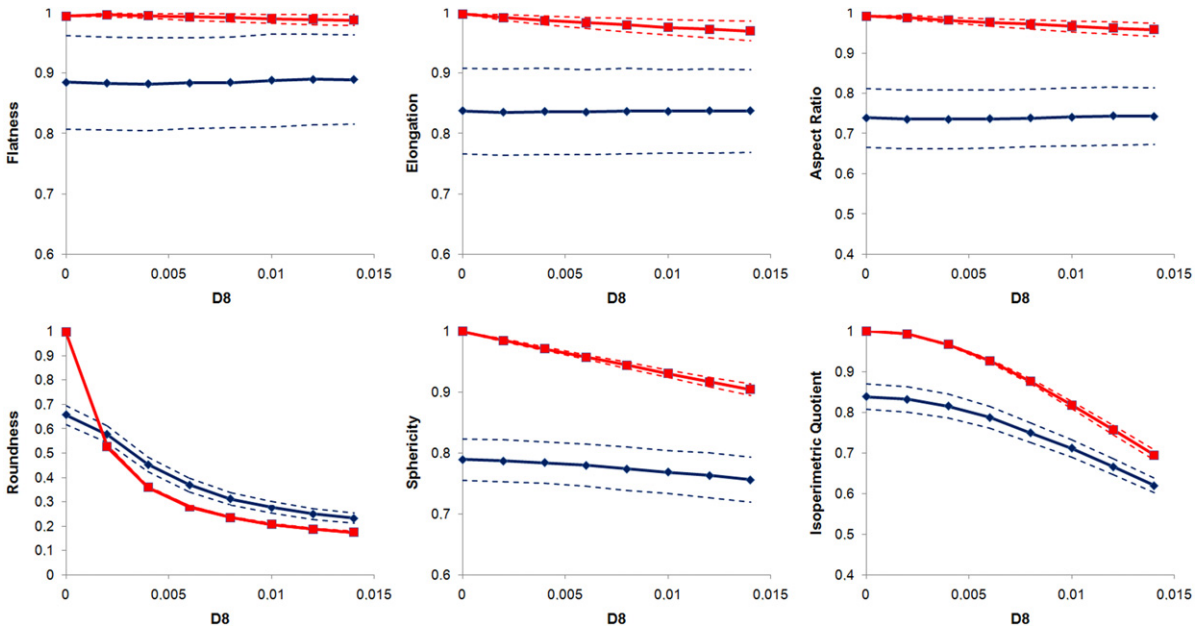

Fig. 9. Influence of the parameter D_8 (modes D_9 and larger being related to D_8 by logarithmic decay) on the Flatness, Elongation, Aspect Ratio, Roundness, Sphericity, and Isoperimetric Quotient of 2000 generated particles. Solid lines: mean values; Dotted lines: mean values $+/-$ one standard deviation. In blue: all other modes consistent with the spectrum of Fig. 6; In red: all other modes set to zeros. (For interpretation of the references to colour in this figure legend, the reader is referred to the web version of this article.)

As expected, Fig. 7 shows that the parameter D_2 has a marked influence on the dimension ratios of the generated shapes (Flatness, Elongation, and Aspect Ratio). Large values of D_2 (such as 0.10–0.15) lead to average values for Flatness and Elongation smaller than 0.75 and the average Aspect Ratios smaller than 0.6, but the dispersions of these ratios increase significantly with D_2. An increase in D_2 also tends to decrease the Sphericity of the generated particles, but has a limited effect on the Isoperimetric Quotient and has negligible effect on the particle Roundness. The influence of the parameter D_3 depicted in Fig. 8 is different, depending on the other modes of the spectrum. If all the other modes (D_2 and $D_{>7}$) are set to be zeros, an increase in D_3 leads to a decrease of all the six shape descriptors, especially the Roundness, the Sphericity and the Isoperimetric Quotient. If the other modes are nonzero, however, its influence on the Flatness, the Elongation, the Aspect Ratio and the Roundness is rather limited. The trends shown in Fig. 9 on the influence of D_8 are easy to tell, since this parameter has no influence on such main dimension ratios as Flatness, Elongation and Aspect Ratio (it only controls the surface roughness), and only shows a limited influence on the Sphericity. An increase in D_8 however leads to a strong decrease of the particle Roundness and its Isoperimetric Quotient.

3. Particles packing

3.1. Constrained Voronoi tessellation

Apart from their generation, the packing of virtual particles in a given container for discrete modelling remains a great challenge for the community. For circular or spherical particles, several geometric methods exist (e.g. [30]), taking advantage of the simplicity of these shapes (especially their invariance by rotation, which makes possible to assume simplified contact detections). For particles with complex shapes, quite often the DEM software is needed to perform this packing directly, because of the complication caused by contact detections and particle positioning. Frequently the DEM is so coded to position the particles on a regular lattice with random orientations and to pack the particles either by gravitational deposition method, isotropic compaction method or by particles inflation (expansion) approach. Using any of these methods, the packing process in DEM may be painfully long (sometimes much longer than the simulation that one wants to perform afterwards) because it requires very loose lattices to ensure that there is no interparticle penetration at the initial state. In our previous 2D study [23], we proposed an alternative method based

on the controlled partition of the virtual container by the means of a Constrained Voronoi Tessellation. This method was inspired by the IMC framework initially appeared in [31]. Voronoi tessellation is a well known useful tool. It generates a random cloud of seeding points in a given domain and then divides this domain into a number of cells according to these seeding points. In its original version, the Voronoi tessellation has no control of the properties of these cells, which, if used directly, may cause some issues in particle packing (see discussion in [23]). A constrained Voronoi tessellation has been proposed in [23] for proper particle packing, which comprises the following steps:

1. Generate an initial set of points within the selected domain, and perform a bounded Voronoi tessellation (i.e. the union of all the cells is identical to the whole domain).
2. Evaluate the desired statistics of the Voronoi tessellation, for example, in terms of size distribution, cells orientations, number of neighbours, etc.
3. Compute an error corresponding to the discrepancy between the current and the target statistics.
4. Move randomly one of the seeding points to another random location, compute the new tessellation, and update the cells statistics.
5. If the error is lower than its previous value, accept the modification; otherwise reject it.
6. Cycle on Steps 4 and 5 until the error has reached an acceptable value.

A number of refinements on the above algorithm are developed in the present work. Specifically, we only perform the stochastic iterative optimization on the size distribution of the Voronoi cells in terms of their volumes. A target probability density function (PDF) of the cell volumes is chosen, based on the desired number of cells, the total volume of the container and the desired dispersion and statistical distribution of these volumes. This PDF is called $pdf_{target}(V)$. Meanwhile, for a given cloud of seeding points, a quick statistical analysis is performed to access the current distribution of the volumes, $pdf_{current}(V)$. The error function to be minimized is then defined as:

$$\text{Error} = \int_0^\infty |pdf_{target}(V) - pdf_{current}(V)|dV. \tag{22}$$

If the target PDF is chosen to describe strictly positive variables (e.g. lognormal distribution), this error is always ranged between 0 and 2, and a target value of 0.1 can provide satisfactory results. In practice, the integral is computed numerically, using discretized versions of the probability density function.

To improve the efficiency of the process, Step 4 of the above algorithm is optimized in the same way as described in [23]: the randomly chosen seeding point is moved somewhere in a domain composed by its own current Voronoi cell and its direct neighbours, and the re-computation of the Voronoi tessellation and of the cells volumes is only performed locally (instead of doing it for all the cells) to save computation time. Despite this coding effort, the convergence may be rather slow, especially when large numbers of seeding points in conjunction with complicated domain geometry and "extreme" volume distributions (i.e. with very small or very large dispersions) are considered. A good way to improve efficiency is to carefully choose the initial cloud of points. Based on efficiency and performance, we recommend a simple uniform random distribution for large target dispersions (i.e. for coefficients of variations larger than 0.4) and a quasi-MC distribution (such as the Halton series, [32]) for low target dispersions. More details on these points are provided in the 2D framework in [23], and similar main concepts are equally applicable to the 3D case. Some illustrative results are provided in Fig. 10, where a unit cube is partitioned into 2000 cells. The target size distributions are lognormal, with coefficients of variations of 0.1, 0.5, and 1.2 from left to right. The target error is 0.1, and the number of cycles (i.e. of motions of seeding points, may they be successful or not) are respectively of 23,800, 162, and 10,800. This indicates that the method is much more efficient for moderate values of size dispersion. While the example demonstrates the robustness of the method, a comparison between the target and obtained volume distributions also proves that it can offer a satisfactory accuracy (lower part of Fig. 10).

3.2. Cell-filling algorithm

Once the virtual domain has been partitioned with the cells of prescribed sizes, we wish to fill each of them with a virtual particle generated from a given Fourier spectrum. In order for the granular sample to reproduce the size distribution imposed during the constrained Voronoi tessellation, the filling process needs to ensure that the same volume fraction is obtained and no part of this particle is outside the cell after the filling. This can be achieved through the following steps. We first analyse the cell by computing the position of its centre of mass and the list of angles

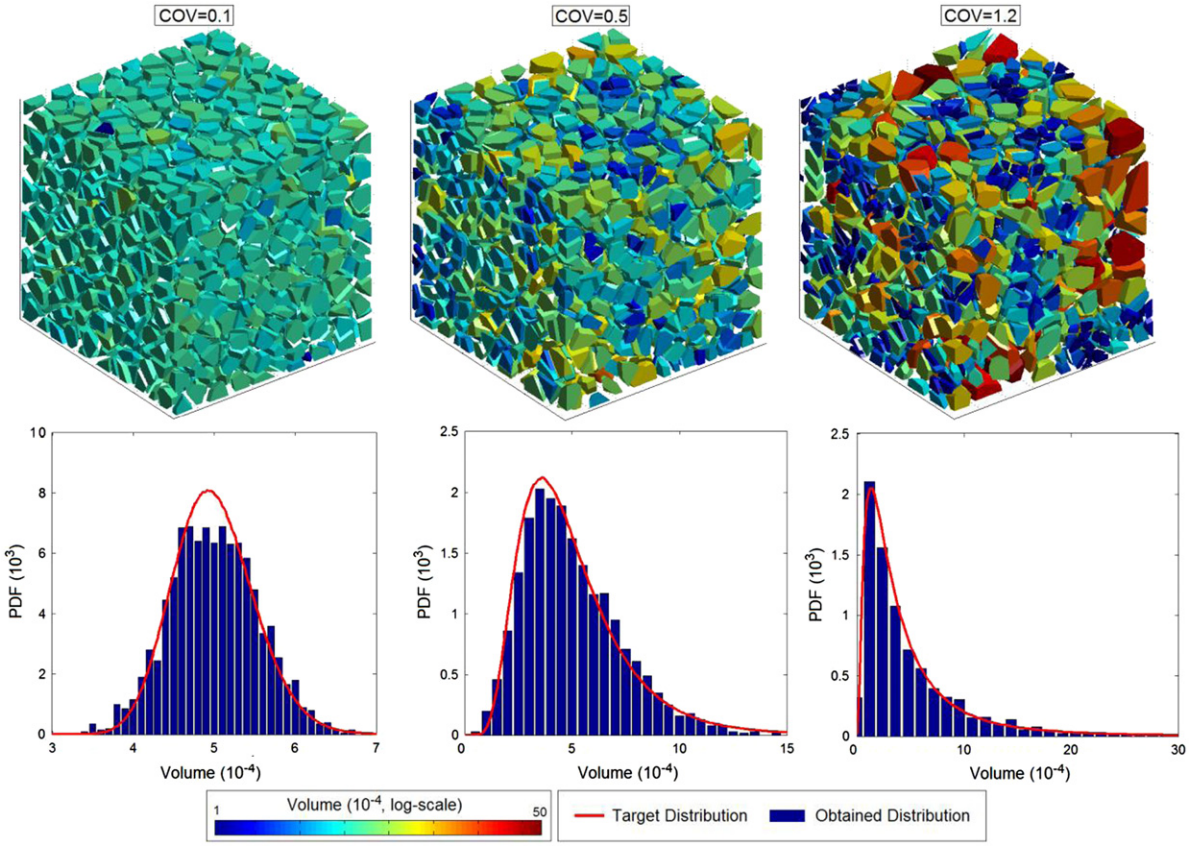

Fig. 10. Constrained Voronoi Tessellation obtained for three target coefficients of variation (COV) of the cells volumes. Top: obtained cells (artificially separated to clarify the figure); Bottom: target and obtained volume distributions.

$\{\theta_i, \varphi_i\}$ of an equivalent geodesic structure (Fig. 3c) with $1 \leq i \leq 2562$. For each of these spatial directions i, the distance $L_{n,i}$ from the centre of mass of cell n to its external surface is computed. We hereby obtain a collection of radiuses $\{L_n\}$ which is analogous to the collection $\{R_n\}$ of radiuses of a particle n, except that it describes the cell contour. A simple way to ensure that the particle is completely located inside the cell is to place its centre at the centre of mass of the cell and to fulfil the following conditions:

$$R_{n,i} \leq L_{n,i} \quad \forall\, i \in [1; 2562]\,. \tag{23}$$

This condition may be ensured by simply dividing all the particle radiuses by a unique factor given by $\max_i \left\{R_{n,i}/L_{n,i}\right\}$ without modifying the particle shape. This operation will lead to the densest state allowed by the method, but smaller solid fractions may be obtained by simply choosing a different scaling factor. When working on a full packing of granular sample, it is advisable to target a solid fraction smaller than the maximal one, so that it can be reached for most of the cells in order to reduce the disturbance of the size distribution of the particles with respect to the one of the cells. Notably, however, no matter what the target solid fraction is, if condition (23) is fulfilled, any contact and/or penetration between particles are prohibited since each particle will be strictly contained in a given cell. This implies that no stress state exists in such a generated sample. To have the sample reach a realistic granular state, a further stage of compaction (either by gravitational deposition or by isotropic compression, for example) may be needed in conjunction with proper contact laws. Therefore, the target solid fraction of the proposed method only provides an indicator of the computational cost needed to reach a proper state of compaction, rather than the actual packing used directly for DEM.

The cell-filling method is demonstrated with illustrative examples in Fig. 11a–c. In these figures one may observe successively a typical polyhedral cell obtained from the constrained Voronoi tessellation, the same cell represented as a geodesic structure after computation of the radiuses $\left\{L_{n,i}\right\}$, and a random particle whose radiuses have been scaled

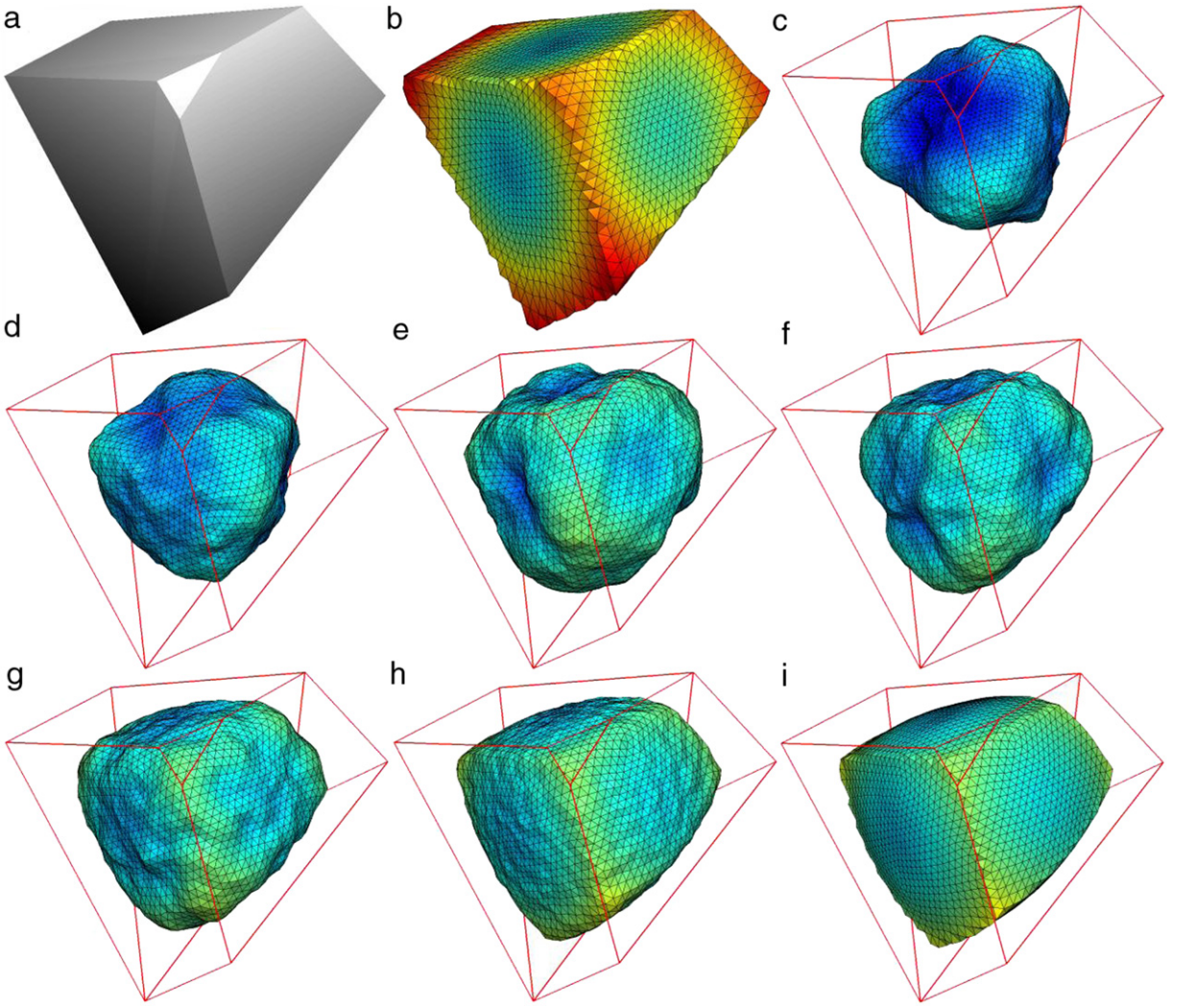

Fig. 11. Cell-filling algorithm: a. Polyhedral cell to be filled; b. Same cell expressed as a geodesic structure; c. Particle filled in cell with $N_{fit} = 0$; d. $N_{fit} = 10$; e. $N_{fit} = 20$; f. $N_{fit} = 50$; g. $N_{fit} = 100$; h. $N_{fit} = 500$; i. $N_{fit} = 2562$.

following Eq. (23). It is clear from this figure that such a method might lead to rather poor filling ratios, since the respective shapes of the cell and the particle do not necessarily have to be similar. This may force one to strongly reduce the size of the particle to have it entirely contained in the cell, and the final packing might be rather loose. To resolve this issue, we propose the following method.

The main idea is to adapt the shape of the particle to the cell to be filled in, without altering the frequential content provided by the input Fourier spectrum. It requires a pre-processing of all the cells of the domain prior to the generation of the particles. Firstly, the radiuses $\{L_n\}$ are computed as in the initial method, for all the directions i and for all cells. For each cell n (with $1 \leq n \leq N$), the radiuses are normalized in order to have a unit mean radius:

$$L'_{n,i} = \frac{2562 \times L_{n,i}}{\sum_{k=1}^{2562} L_{n,k}} \quad \forall\, i \in [1; 2562]\,. \tag{24}$$

Each one of these "normalized cells" is then projected in the eigenspace defined by the covariance matrix $\left[C'\right]$, using the eigenvectors $\left\{\Phi_j\right\}$ of this matrix. Defining the matrix $[\Phi]$ (each column of which being one of the eigenvectors $\left\{\Phi_j\right\}$), of generic term Φ_{ij} (with j being the index of the eigenmode and i being the line index), the projection of the

normalized cell n on a given mode j is given by the following inner product:

$$\kappa_{n,j} = \sum_{i=1}^{2562} L'_{n,i} \cdot \Phi_{ij}. \tag{25}$$

With these operations, each normalized cell n may be reconstructed using the following expression:

$$\left\{L'_n\right\} = \{\mu\} + \sum_{j=1}^{2562} \kappa_{n,j} \cdot \left\{\Phi_j\right\}. \tag{26}$$

In this expression, $\{\mu\} = \{1\}$ is a 2562×1 unit vector and $\left\{L'_n\right\}$ is the 2562×1 vector of the normalized radiuses of the cell n. Eq. (26) shares a strong similarity with the formula of the EOLE method used to generate a random particle n:

$$\{R_n\} = \{\mu\} + \sum_{j=1}^{2562} \xi_{n,j} \cdot \sqrt{\lambda_j} \cdot \left\{\Phi_j\right\}. \tag{27}$$

Thus, each cell may be considered as a particle which would have been generated in the way described in Section 2, with a set of coefficients $\{\xi\}$ given by:

$$\xi'_{n,j} = \frac{\kappa_{n,j}}{\sqrt{\lambda_j}}. \tag{28}$$

The collections of coefficients $\xi'_{n,j}$ so defined do not have any reason to be normally distributed with zero mean and unit variance, which is the reason why the cells and the particles have rather different shapes. However, based on this observation, it is also possible to generate virtual particles with shapes similar to the desired cells but still consistent with the desired Fourier spectrum, by simply normalizing the variables $\xi'_{n,j}$. Indeed, if M_j is the average of the variables $\xi'_{n,j}$ over the n particles and Σ_j is their standard deviation, each coefficient $\xi'_{n,j}$ may be replaced by:

$$\xi''_{n,j} = \frac{\xi'_{n,j} - M_j}{\Sigma_j}. \tag{29}$$

Due to this normalization, the coefficients $\xi''_{n,j}$ of a given eigenmode j are distributed over the N particles with a zero-mean and a unit variance. Based on $\xi''_{n,j}$, it is possible to reconstruct the particles which are consistent with the input Fourier spectrum and meanwhile have shapes similar to the desired cells:

$$\{R_n\} = \{\mu\} + \sum_{j=1}^{2562} \xi''_{n,j} \cdot \sqrt{\lambda_j} \cdot \left\{\Phi_j\right\}. \tag{30}$$

An example is provided in Fig. 11i. The obtained shape is apparently different from the one in Fig. 11c, though the same input spectrum and coefficients with zero-mean and unit-variance are used for both. Indeed, these two shapes have the same frequential content (i.e. the same modes with the same amplitudes), but the specific choice of the coefficients $\xi''_{n,j}$ for Fig. 11i leads to a specific alignment of the shape irregularities and to this "facetted" shape, while a completely random choice of the coefficients for Fig. 11c leads to a random orientation of the irregularities. In a certain way, the particle of Fig. 11i has been "fitted" to a target cell, and will thus lead to a larger filling ratio and to a denser granular packing. Though the surface roughness diminution is noticeable, all the high-frequency content is concentrated at the edges of this facetted shape.

An additional degree of freedom may be brought in by using both the fitted coefficients $\xi''_{n,j}$ and the random coefficients $\xi_{n,j}$ in the computation of the particle shape performed in Eq. (27), using the following formula:

$$\{R_n\} = \{\mu\} + \sum_{j=1}^{N_{fit}} \xi''_{n,j} \cdot \sqrt{\lambda_j} \cdot \left\{\Phi_j\right\} + \sum_{j=N_{fit}+1}^{2562} \xi_{n,j} \cdot \sqrt{\lambda_j} \cdot \left\{\Phi_j\right\}. \tag{31}$$

If only the first N_{fit} eigenmodes are fitted (coefficients $\xi''_{n,j}$ for $1 \leq j \leq N_{fit}$), and the others are random (coefficients $\xi_{n,j}$ for $N_{fit} < j \leq 2562$), then one should expect the particle to have a general shape similar to the target cell

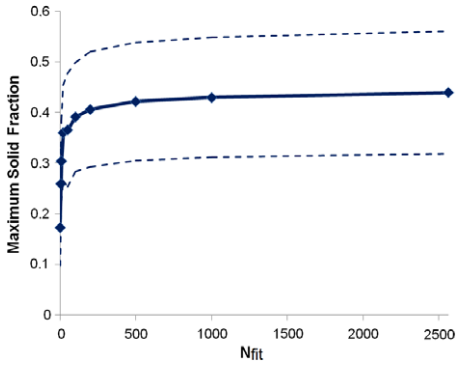

Fig. 12. Influence of N_{fit} on the maximum solid fraction of a 2000 particles packing performed with the illustrative Fourier spectrum of Fig. 6. Solid lines: mean values; Dotted lines: mean values +/− one standard deviation.

(since this global shape is controlled by the first modes), but to keep some randomness in the smaller irregularities and in the surface roughness (which are controlled by the higher modes). Such shapes are provided in Fig. 11d–h, showing all the possible compromises between a completely random shape (Fig. 11c) and a completely fitted shape (Fig. 11i). As expected, increasing the value of N_{fit} leads to a smaller shape randomness and brings an interesting control on the facetted character of the generated particle. It also progressively increases the similarity between the particle and the cell, making it possible to pack the particles with a larger density. This is clearly shown in Fig. 12, for which several packings of 2000 particles have been performed in a unit cube. The input spectrum is the illustrative one already used in Fig. 6, and the value of N_{fit} is varied from 0 to 2562. The influence of this parameter on the maximum packing density is evident. Considering $N_{fit} = 20$ leads to a maximum solid fraction equal to 0.36, which is more than twice the one obtained with completely random shapes ($N_{fit} = 0$). For values of N_{fit} larger than 100, the influence of this parameter becomes rather limited because the higher modes do not have any important effect on the global particle shapes.

In Fig. 13 the same samples with varying values of N_{fit} are considered, and the six shapes descriptors of Eqs. (16)–(21) are computed and plotted in terms of their means and standard deviations as functions of N_{fit}. It appears that N_{fit} seems to have a very limited effect on the shape descriptors, especially beyond 100 fitted modes. In any case, the influence of N_{fit} is much smaller than the ones of D_2, D_3 and D_8 described in Figs. 7–9. This observation is strikingly surprising, since Fig. 11 clearly shows that the parameter N_{fit} strongly affects the visual appearance of particles. It means that the six shape descriptors used in this paper are mostly controlled by the amplitudes of the modes of the input Fourier spectrum, but are rather independent from the way these modes are organized around the particle (i.e. they do not depend on the fact that the irregularities are concentrated on edges and define facets). Hence, a quantitative geometric descriptor characterizing the "facetted" character of a particle is probably still lacking to characterize the influence of the parameter N_{fit}.

4. Conclusions and discussion

In this study, we developed a systematic statistical framework for the generation of virtual 3D particles with realistically complex and controllable shapes and for packing them effectively for use in discrete-element modelling of granular materials. The theory of random fields and a Fourier-shape-descriptor based method previously proposed by the authors are combined for the particle generation. The generated particles are then packed within a prescribed container by a cell-filling algorithm based on Constrained Voronoi Tessellation. Demonstrated by examples, the proposed methods offer good control and great flexibility in reproducing such key characteristics as shape descriptors (aspect ratio, roundness, sphericity, presence of facets, etc.), size distribution and solid fraction. Being developed in a general and robust manner, the proposed framework is not only useful for discrete element method modelling, it can also be implemented for any other particle-based approaches where the physical attributes of the particles are important.

The various methods described in this paper have been implemented into a single program pack called "Packing3D", coded in MATLAB and made available for free download at the URL http://guilhem.mollon.free.fr. The input parameters of this program are the geometry of the container, the number of particles, the desired statistical distribution

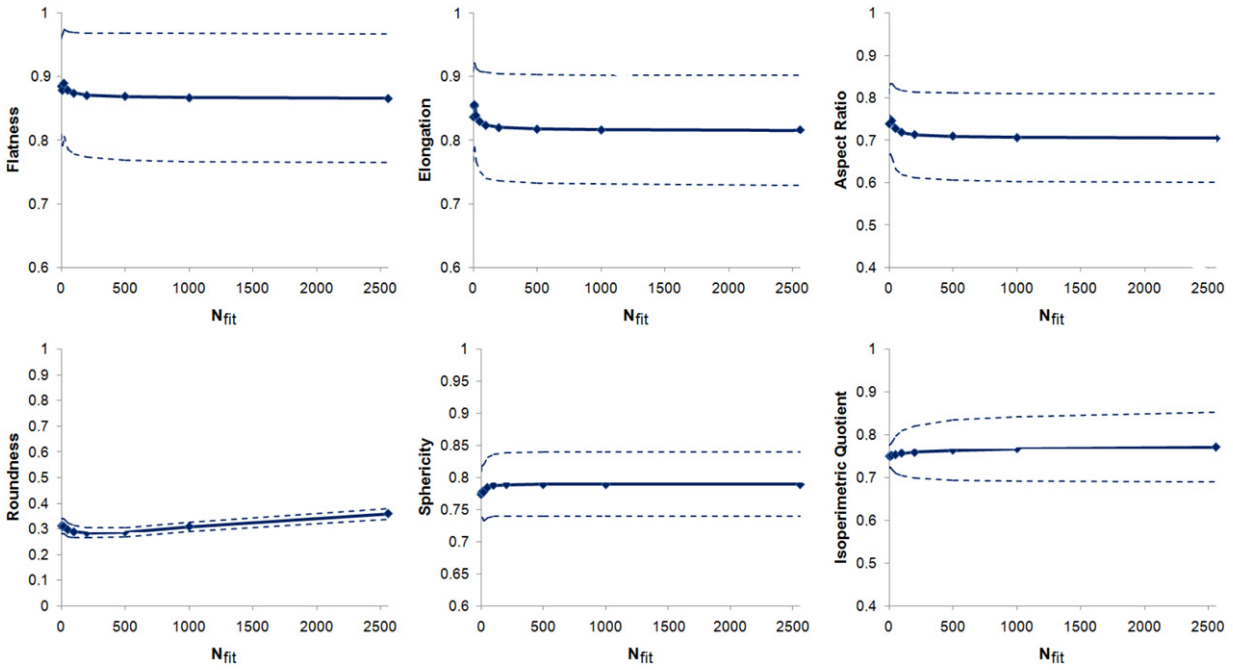

Fig. 13. Influence of N_{fit} on the Flatness, Elongation, Aspect Ratio, Roundness, Sphericity, and Isoperimetric Quotient of a 2000 particles packing performed with the illustrative Fourier spectrum of Fig. 6. Solid lines: mean values; Dotted lines: mean values +/− one standard deviation.

of their volumes, the desired solid fraction, the Fourier spectrum, and the number of eigenmodes of the particles to be fitted on the Voronoi cells. Based on these inputs, the program will follow several successive major steps:

- Perform a constraint Voronoi tessellation of the container in a desired number of polyhedral cells with the desired volume dispersion and distribution.
- Compute the corrected covariance matrix $\left[C'\right]$, its eigenvectors $\left\{\Phi_j\right\}$ and its eigenvalues λ_j, based on the stored correlation matrices $\left[\rho'\right]_K$ of each Fourier mode K and on the input Fourier spectrum.
- Express each Voronoi cell in terms of the normalized radiuses $\left\{L'_n\right\}$, project them in the eigenspace of the covariance matrix in terms of the coefficients $\kappa_{n,j}$, and compute the equivalent coefficients $\xi'_{n,j}$. For each eigenmode j, evaluate the mean and the standard deviation of these coefficients over the N particles, and normalize them to obtain the fitted coefficients $\xi''_{n,j}$ with zero-mean and unit-variance.
- Use Eq. (31) to compute the radiuses of each of the N particles, accounting for the desired number of fitted and random eigenmodes.
- Place the generated particles in their respective cells and scale them with respect to the target solid fraction, or with respect to the condition of Eq. (23) if it is not fulfilled.

Regarding the computational efficiency of the proposed algorithm, the influencing factors include the total number of particles and the desired dispersion of the particles volumes. For very small (e.g. 0.1) or very large (e.g. 1.2) coefficients of variations of the volumes, the computation of constrained Voronoi tessellation may be costly and constitutes the majority of the computational time, while for moderate value (e.g. 0.3–0.7) cases, this stage is rather fast and the main time cost is spent on the description of the cells in terms of the collections of radiuses $\{L_n\}$, since this process requires a very large number of geometric computations. Two examples are provided in Fig. 14, further demonstrating the interesting flexibility of the proposed framework. The left-hand one corresponds to the packing of 2500 sand particles in a cylindrical container, while the right-hand one corresponds to the packing of 1000 pebbles in an octagonal hopper. The sand sample has a rather large size distribution with grains of complex shapes and rough surfaces without noticeable facets, while the pebbles have a rather narrow size distribution and a smooth surface with a noticeable facetted character. From top to bottom, Fig. 14 provides for each sample a zoomed view of a few particles, a global view of the sample (the colour of each particle denoting its volume), and a confrontation between the targeted and obtained values/distributions of particles volume, aspect ratio, roundness and sphericity. The input

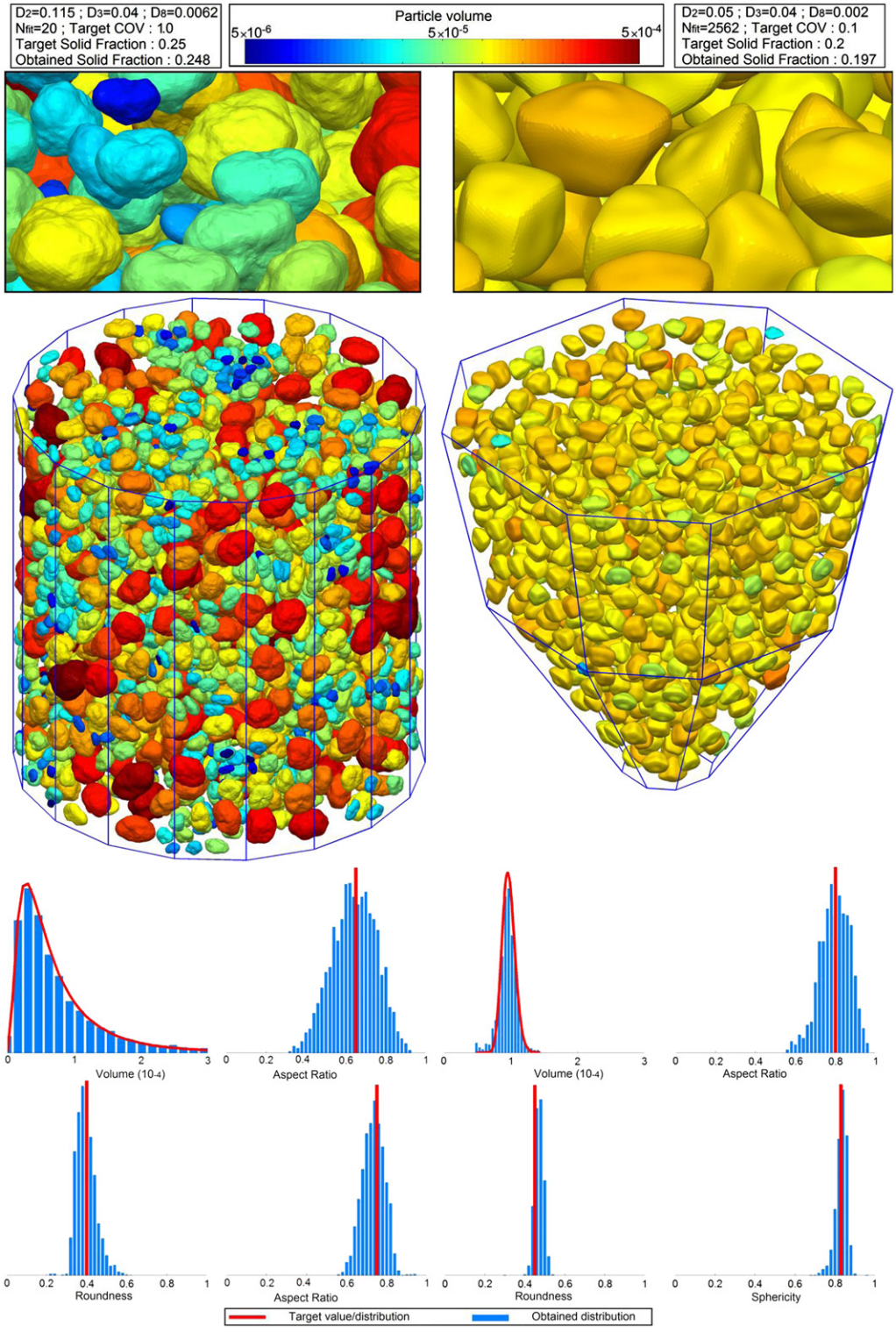

Fig. 14. Two examples of generated granular samples.

Fourier spectrums (controlled in this case by the parameters D_2, D_3 and D_8) and the number of fitted modes N_{fit} were calibrated by trial-and-error using a smaller sample of 100 particles in a module of the MATLAB code devoted to this task (and for a limited time cost) to match the target values of aspect ratio, roundness and sphericity plotted in red in the lower graphs. Clearly shown with the great flexibility and good control from Fig. 14, the proposed framework offers the capacity to cover a majority of granular materials that are commonly encountered in scientific and industrial applications.

A major challenge in continuing this line of the present work will be to set up a methodology of calibration on the Fourier spectrum and the number of fitted eigenmodes N_{fit} to reproduce accurately the morphology of a real granular material. The approach we used in [27] was based on the contour analysis of the scanning electron micrographs of particles. This method does not seem to be robust enough since it requires extrapolating 3D shapes from 2D pictures, which may introduce some arbitrariness. A complete statistical analysis of 3D real shapes of particles might be necessary, including their dimensions ratios, main irregularities and surface roughness, as well as the facetted character of the particles (which so far lacks a robust quantitative descriptor), as well as some other unknown shape descriptors. To this end, accurate and effective experimental acquisitions of real 3D shapes of the target particles might be necessary for this calibration. Possible solutions may be provided with the recent progress in X-ray computed micro-tomography and particle tracking algorithms [33]. When this difficulty is overcome, the predictive ability of DEM based on the realistic particles can then be benchmarked with the experimental results. Prior to that, an effective strategy to introduce the complex particles into a DEM code is still needed. The candidate approaches include overlapping spheres (ODECS, see [3]), polyhedrons [18], sphero-polyhedrons [20], or the recent NURBS technique [34]. Understandably, accounting for particles with such complexity in shape as described in the paper may demand important computational costs that might be beyond the capacity of common computers. For example, an affordable ODECS technique may need 100–400 spheres to represent the contour of a single particle, with which the fine surface details of the particle (e.g., roughness) may not be properly reproduced. The NURBS techniques are still under development where the handling of multi-contacts may still have to be made robust enough. The polyhedron and sphero-polyhedron methods seem to be robust enough, but are most computationally expensive among these methods. If the geometrical calibration is successful, more effort will have to be paid to the choice and calibration of the contact law too (as was done in [21], for example). For example, it remains an open question whether or not an equivalent adjustment of the friction coefficient can be made to replace the high-frequency modes of roughness without altering the behaviour of the granular material. Only when all these steps are accomplished can the DEM be considered predictive in providing reliable quantitative results without back-analysis-based calibration.

References

[1] P.A. Cundall, O.D.L. Strack, A discrete numerical model for granular Assemblies, Geotechnique 29 (1979) 47–65.
[2] P.A. Thomas, J.D. Bray, Capturing nonspherical shape of granular media with disk clusters, J. Geotech. Geoenviron. Eng. 125 (1999) 169–178.
[3] J.-F. Ferellec, G. McDowell, A method to model realistic particle shape and inertia in DEM, Granular Matter 12 (2010) 459–467.
[4] G. Mollon, J. Zhao, Characterization of fluctuations in granular hopper flows, Granular Matter 15 (6) (2013) 827–840.
[5] R.P. Jensen, T.B. Edil, P.J. Bosscher, M.E. Plesha, N. Ben Kahla, Effect of particle shape on interface behavior of DEM-simulated granular materials, Int. J. Geomech. 1 (1) (2001) 1–19.
[6] M. Stahl, H. Konietzky, Discrete element simulation of ballast and gravel under special consideration of grain-shape, grain-size and relative density, Granular Matter 13 (2011) 417–428.
[7] J. Katagiri, T. Matsushima, Y. Yamada, Simple shear simulation of 3D irregularly-shaped particles by image-based DEM, Granular Matter 12 (2010) 491–497.
[8] T. Matsushima, J. Katagiri, K. Uesugi, A. Tsuchiyama, T. Nakano, 3D shape characterization and image-based DEM simulation of the Lunar soil simulant FJS-1, J. Aerospace Eng. 22 (1) (2009) 15–23.
[9] G. McDowel, H. Li, I. Lowndes, The importance of particle shape in discrete-element modelling of particle flow in a chute, Géotech. Lett. 1 (3) (2011) 59–64.
[10] P. Fu, Y. Dafalias, Fabric evolution within shear bands of granular materials and its relation to critical state theory, Int. J. Num. Anal. Meth. Geomech. 35 (18) (2011) 1918–1948.
[11] X. Lin, T.T. Ng, A three-dimensional discrete element model using arrays of ellipsoids, Géotechnique 47 (2) (1997) 319–329.
[12] T.-T. Ng, Particle shape effect on macro- and micro-behavior of monodisperse ellipsoids, Int. J. Num. Anal. Meth. Geomech. 33 (2009) 511–527.
[13] H. Ouadfel, L. Rothenburg, "Stress-force fabric" relationship for assemblies of ellipsoids, Mech. Mater. 33 (2001) 201–221.
[14] L. Pournin, M. Weber, M. Tsukahara, J.-A. Ferrez, M. Ramaioli, T.M. Liebling, Three-dimensional distinct element simulation of spherocylinder crystallization, Granular Matter 7 (2) (2005) 119–126.
[15] H.-J. Tillemans, H.-J. Herrmann, Simulating deformations of granular solids under shear, Phys. Rev. A 217 (1995) 261–288.

[16] A.A. Pena, R. Garcia-Rojo, H.J. Herrmann, Influence of particle shape on sheared dense granular media, Granular Matter 9 (2007) 279–291.
[17] M. Lu, G.R. McDowell, The importance of modelling ballast particle shape in DEM, Granular Matter 9 (2) (2007) 71–82.
[18] E. Azema, F. Radjai, G. Saussine, Quasistatic rheology, force transmission and fabric properties of a packing of irregular polyhedral particles, Mech. Mater. 41 (2009) 729–741.
[19] S.-A. Galindo-Torres, D.-M. Pedroso, Molecular dynamics simulations of complex-shaped particles using Voronoi-based spheropolyhedra, Phys. Rev. E 81 (2010) 061303.
[20] S.-A. Galindo-Torres, J.-D. Munoz, F. Alonso-Marroquin, Minkowski-Voronoi diagrams as a method to generate random packing of spheropolygons for the simulation of soils, Phys. Rev. E 82 (2010) 056713.
[21] V. Richefeu, G. Mollon, D. Daudon, P. Villard, Dissipative contacts and realistic block shapes for modelling rock avalanches, Eng. Geol. 19 (150) (2012) 78–92.
[22] G. Mollon, V. Richefeu, P. Villard, D. Daudon, Numerical simulation of rock avalanches: influence of a local dissipative contact model on the collective behavior of granular flows, J. Geophys. Res. Solid Earth 117 (2013) F02036.
[23] G. Mollon, J. Zhao, Fourier–Voronoi-based generation of realistic samples for discrete modelling of granular materials, Granular Matter 14 (2012) 621–638.
[24] E.T. Bowman, K. Soga, W. Drummond, Particle shape characterization using Fourier descriptor analysis, Geotechnique 51 (6) (2001) 545–554.
[25] N. Das, Modeling Three-dimensional Shape of Sand Grains Using Discrete Element Method (Ph.D. thesis) University of South Florida, 2007.
[26] G. Mollon, J. Zhao, The influence of particle shape on granular hopper flow, Powders and Grains 2013, AIP Conf. Proc. 1542 (2013) 690–693.
[27] G. Mollon, J. Zhao, Generating realistic 3D sand particles using Fourier descriptors, Granular Matter 15 (1) (2013) 95–108.
[28] C.C. Li, A. Der Kiureghian, Optimal discretization of random fields, J. Eng. Mech. 119 (6) (1993) 1136–1154.
[29] S.J. Blott, K. Pye, Particle shape: a review and new methods of characterization and classification, Sedimentology 55 (2008) 31–63.
[30] J.-F. Jerier, D. Imbault, F.-V. Donze, P. Doremus, A geometric algorithm based on tetrahedral meshes to generate a dense polydisperse sphere packing, Granular Matter 11 (2009) 43–52.
[31] D. Gross, M. Li, Constructing microstructures of poly- and nanocrystalline materials for numerical modeling and simulation, Appl. Phys. Lett. 80 (5) (2002) 746–748.
[32] J. Halton, Algorithm 247: radical-inverse quasi-random point sequence, Comm. ACM. 7 (12) (1964) 701.
[33] S.A. Hall, M. Bornert, J. Desrues, Y. Pannier, N. Lenoir, G. Viggiani, P. Bésuelle, Discrete and continuum analysis of localised deformation in sand using X-ray μCT and volumetric digital image correlation, Géotechnique 60 (5) (2010) 315–322.
[34] J.E. Andrade, K.W. Lim, C.F. Avila, I. Vlahnich, Granular element for computational particle methods, Comput. Methods Appl. Mech. Engrg. 241–244 (2012) 262–274.